Riccardo Fantoni and Andrés Santos

Depletion force in the infinite-dilution limit in a solvent of nonadditive hard spheres

Riccardo Fantoni[1,a)] and Andrés Santos[2,b)]

[1]*Dipartimento di Scienze dei Materiali e Nanosistemi, Università Ca' Foscari Venezia, Calle Larga S. Marta DD2137, I-30123 Venezia, Italy*

[2]*Departamento de Física and Instituto de Computación Científica Avanzada de Extremadura (ICCAEx), Universidad de Extremadura, Badajoz E-06071, Spain*

The mutual entropic depletion force felt by two solute "big" hard spheres immersed in a binary mixture solvent of nonadditive "small" hard spheres is calculated as a function of the surface-to-surface distance by means of canonical Monte Carlo simulations and through a recently proposed rational-function approximation [R. Fantoni and A. Santos, Phys. Rev. E **84**, 041201 (2011)]. Four representative scenarios are investigated: symmetric solute particles and the limit where one of the two solute spheres becomes a planar hard wall, in both cases with symmetric and asymmetric solvents. In all cases, the influence on the depletion force due to the nonadditivity in the solvent is determined in the mixed state. Comparison between results from the theoretical approximation and from the simulation shows a good agreement for surface-to-surface distances greater than the smallest solvent diameter. © 2014 AIP Publishing LLC. [http://dx.doi.org/10.1063/1.4884353]

I. INTRODUCTION

In chemical physics, one often finds solute particles immersed in a solvent. Even though the solute particles interact through a *true* potential, an important problem consists of reducing the solute-solvent system of particles to an equivalent one made of only the solute particles but interacting through an *effective* potential. This problem has been much studied for the paradigmatic case of an athermal mixture of additive hard spheres (AHS)[1] and for the more general case of nonadditive hard spheres (NAHS).[2–4] The problem is usually solved in a two-step procedure. Starting from the pioneering work of Asakura and Oosawa,[5] one first determines the effective *pair* potential, the so-called *depletion entropic potential*, between *two* "big" solute hard spheres (in three[6–8] or two[9] dimensions) immersed in a solvent of "small" hard spheres. Once this stage has been carried out, one can study the properties of a fluid of particles interacting with such an effective pair potential.[10] While the assumption of pairwise additivity is essentially uncontrolled, since the presence of a third particle in the vicinity of a pair of solutes will alter the solvent (the depletant) spatial distribution, it is expected that such limitations of the pairwise additivity approximation become progressively less relevant on decreasing the solute density and/or the size ratio between the diameter of a solvent particle and that of a solute particle. The oscillations in the depletion potential, for example, are found to be responsible for gelation in binary mixture of hard spheres[11] and for spatial heterogeneity in bimodal colloidal suspensions.[12]

In the present work, we are interested in the first step of such a programme. The depletion potential problem has been studied in several different scenarios. One can have nonspherical solute[13] or solvent[14] particles. For spherical solute and solvent particles, the case we are interested in, the solvent itself may be an AHS mixture (binary,[15] multicomponent,[16] or polydisperse[17,18]). Additionally, the solvent particles may have various kinds of interaction.[19–22] When the solvent particles interact with a potential which has some attraction, an interesting issue is the one of understanding how the depletion or force will be affected upon approaching the gas-liquid coexistence critical point of the solvent, where the critical fluctuations are expected to give rise to the so-called thermodynamic Casimir forces.[23–26]

Recently, we constructed an approximate theory for the structure and the thermodynamics of a general NAHS multicomponent mixture,[27,28] which we called the (first order) rational-function approximation (RFA). The theory provides a fully analytical representation of the radial distribution functions in Laplace space which extends to the nonadditive case the exact solution of the Percus–Yevick (PY) integral equation for AHS mixtures.[29,30] It is the purpose of the present work to use the RFA theory to predict the depletion force when the solvent is a NAHS binary mixture and to compare our theoretical predictions with Monte Carlo (MC) simulation results. We clearly want to avoid demixing[31,32] in the solvent. This restricts the combinations of solvent density and (positive) nonadditivity that we are allowed to choose. An interesting open problem, that we leave to a future study, is the study of how the depletion force is affected by approaching the demixing critical point on the critical isochore.

In order to find the depletion force in the simulations, we followed the MC method of Dickman *et al.*[33] In molecular dynamics simulations, however, a different strategy[34] is more suitable. We decided not to determine the depletion potential from the force because the spatial integration of the latter can introduce additional uncontrolled uncertainties. On

---

a)Electronic mail: rfantoni@ts.infn.it

b)Electronic mail: andres@unex.es. URL: http://www.unex.es/eweb/fisteor/andres/.

140, 244513-1

the other hand, it is possible to determine the depletion potential directly in a MC simulation by allowing the two solute impurities to move.[26]

We will consider four different scenarios: (i) two symmetric solute particles in a symmetric solvent, (ii) two symmetric solute particles in an asymmetric solvent, (iii) extremely asymmetric solutes, in the limit where one of the two solute spheres reduces to a planar hard wall,[28] in a symmetric solvent, and (iv) the same situation but in an asymmetric solvent.

The paper is organized as follows. In Sec. II, we introduce the fluid model we set up to study further on, while in Sec. III the observable to be measured in MC simulations and estimated with our RFA theory is described. Details about our MC simulations are given in Sec. IV. Section V presents the numerical and theoretical results for the depletion force and compares them. The paper is closed in Sec. VI with some final remarks.

II. THE MODEL

We consider the following general model. Two solute big hard spheres (the impurities) of species a and b and diameters $\sigma_a = \sigma_{aa}$ and $\sigma_b = \sigma_{bb}$ with $\sigma_{ab} = \frac{1}{2}(\sigma_a + \sigma_b)$ are immersed in a NAHS binary mixture solvent made of N_μ small hard spheres of species $\mu = 1, 2$ of diameter $\sigma_\mu = \sigma_{\mu\mu}$ in a volume V, such that

$$\sigma_{12} = \frac{\sigma_1 + \sigma_2}{2}(1 + \Delta) \qquad (2.1)$$

with $\Delta > -1$ measuring the solvent nonadditivity. The solute-solvent interaction is assumed to be additive, i.e., $\sigma_{\mu\alpha} = \frac{1}{2}(\sigma_\mu + \sigma_\alpha)$ with $\mu = 1, 2$ and $\alpha = a, b$.

Without loss of generality, we take $\sigma_1 (\leq \sigma_2)$ as length unit. Thus, we define the solvent/solvent size ratio $\sigma_2/\sigma_1 \geq 1$, the solute/solute size ratio $\sigma_b/\sigma_a \geq 1$, and the solute/solvent size ratio $\sigma_a/\sigma_1 > 1$. The solvent total number density is $\rho = N/V = \sum_{\mu=1}^2 N_\mu/V = \sum_{\mu=1}^2 \rho_\mu$ and the mole fraction of species $\mu = 1, 2$ is $x_\mu = \rho_\mu/\rho$, with $x_1 + x_2 = 1$. From this we can introduce the partial packing fractions $\eta_\mu = \frac{\pi}{6}\rho x_\mu \sigma_\mu^3$ and the nominal total packing fraction $\eta = \sum_\mu \eta_\mu$.

The model is characterized by the following set of six independent dimensionless parameters: η, x_1, σ_2/σ_1, and Δ, defining the solvent, and σ_b/σ_a and σ_a/σ_1, defining the solute. Note that the model can also be obtained from the more general one of a quaternary mixture with $a = 3$, $b = 4$ in the limit of infinite solute dilution $x_3 \to 0$, $x_4 \to 0$.[7]

The depletion force is formally independent of the solvent-solvent interaction (see Sec. III).[33,35] But of course it depends on the *local* solvent density in the neighborhood of the solute particles and such a density is affected by the solvent-solvent and solvent-solute interactions. A natural question then arises: As the solvent-solvent nonadditivity is switched on, how the induced change in the local solvent density affects the depletion force? Clearly, far away from the solute spheres there will be no change in the almost constant local density, i.e., the bulk density. But the local density in the vicinity of the solute particles would change and thereby so would the force. To first order in density, however, the de-

pletion force is completely independent of the solvent-solvent interaction,[7] so the influence of nonadditivity is absent. Thus, one can expect the effect to be small for dilute solvents but its impact as the bulk solvent density increases is uncertain.

We could alternatively switch on a solute-solvent nonadditivity,[2,4,36] but this case is somewhat less interesting than the previous one. For example, in the case of two solute spheres of diameter σ_a immersed in a one-component solvent of spheres of diameter σ_1 with $\sigma_{1a} \neq \frac{1}{2}(\sigma_1 + \sigma_a)$, one can map the problem onto an additive one where the solute particles have an effective diameter $\sigma_a^{\text{eff}} = 2\sigma_{1a} - \sigma_1$, provided that $\sigma_{1a} \geq \frac{1}{2}\sigma_1$. The effective problem determines the depletion force for $r > \sigma_a^{\text{eff}}$, so that the original problem becomes completely solved in the case of negative nonadditivity (since then $\sigma_a > \sigma_a^{\text{eff}}$), while in the case of positive nonadditivity it only remains unsolved in the region $\sigma_a < r < \sigma_a^{\text{eff}}$. For this reason, we will not consider solute-solvent nonadditivity in our analysis.

In this study, we will first restrict ourselves to the particular case of equal solute impurities ($\sigma_b/\sigma_a = 1$) and consider both a symmetric ($\sigma_2/\sigma_1 = 1$, $x_1 = \frac{1}{2}$) and an asymmetric ($\sigma_2/\sigma_1 \neq 1$, $x_1 \neq \frac{1}{2}$) nonadditive solvent. Our aim is to assess in both cases the effect of the solvent nonadditivity on the depletion force. Then, we will consider the case of extremely asymmetric solute impurities in the limit $\sigma_b/\sigma_a \to \infty$, where one of the two impurities is seen as a hard planar wall both by the other solute sphere and by the solvent species.

III. THE DEPLETION FORCE

We want to determine the force exerted on one big solute sphere immersed in a solvent of small spheres due to the presence of a second big solute sphere, assuming a hard-core repulsion between the solvent and the solute. The solvent in the presence of only one solute sphere at the origin will keep being an isotropic fluid (even if not homogeneous anymore) and the solute sphere will feel a zero net force. However, if we add a second solute sphere in the solvent, the isotropy symmetry will be broken (we are then left with a solvent fluid with axial symmetry around the axis connecting the centers of the two solute spheres) and, as a consequence, each solute sphere will exert an effective force $\mathbf{F}$ on the other one, mediated by the solvent. This force has the form[35]

$$\beta \mathbf{F}(r) = -\int_S dA\, \rho^{(r)}(\mathbf{r}_s)\widehat{\mathbf{n}}, \qquad (3.1)$$

where $\beta = 1/k_B T$ is the inverse temperature parameter, the integral is carried out over the surface S of the sphere centered on the solute particle experiencing the force, dA is an elementary area on S, $\widehat{\mathbf{n}}$ is the outward normal unit vector, and $\rho^{(r)}(\mathbf{r}_s)$ is the local density of the solvent (in the presence of the two solute spheres) at the point $\mathbf{r}_s$ on the surface S.

A. Monte Carlo implementation

1. One-component solvent

Let us first assume a one-component solvent made of N spheres of diameter σ_1 and coordinates $\mathbf{r}_i$ ($i = 1, \ldots, N$) in

a volume V. The solute particle of species a is centered at $\mathbf{r}_a$ and the solute particle of species b is centered at $\mathbf{r}_b = \mathbf{r}_a + r\widehat{\mathbf{r}}$. According to Eq. (3.1), the force $\mathbf{F}_{ab}(r) = F_{ab}(r)\widehat{\mathbf{r}}$ felt by sphere b due to the presence of sphere a is then[35]

$$\beta F_{ab}(r) = -\sigma_{1b}^2 \int d\Omega_s \, \cos\theta_s \rho^{(r)}(\mathbf{r}_b + \sigma_{1b}\widehat{\mathbf{s}}), \quad (3.2)$$

where $d\Omega_s = \sin\theta_s d\theta_s d\varphi_s$ is the elementary solid angle spanned by $\widehat{\mathbf{s}}$ taking the polar axis along $\widehat{\mathbf{r}}$, $\rho^{(r)}(\mathbf{q}) = \langle \sum_i \delta(\mathbf{q} - \mathbf{r}_i) \rangle$ is the local density of the solvent in the presence of the two solute spheres at a center-to-center distance r, and $\langle \cdots \rangle$ is a thermal average.

The expression (3.2) for the depletion force is formally independent of the interaction between the solvent particles and holds as long as we have a hard-sphere interaction between the solvent and the two solute spheres. Clearly, due to the axial symmetry of the solvent fluid, $\rho^{(r)}(\mathbf{r}_b + \sigma_{1b}\widehat{\mathbf{s}}) = \langle \sum_i \delta(\sigma_{1b}\widehat{\mathbf{s}} - \mathbf{s}_i) \rangle$, with $\mathbf{s}_i = \mathbf{r}_i - \mathbf{r}_b$, is a function of σ_{1b} and θ_s only. Notice that, by Newton's third law, we must have $F_{ab} = -F_{ba}$. In terms of the potential of mean force $\beta u_{ab}(r) = -\ln g_{ab}(r)$, where $g_{ab}(r)$ is the solute-solute radial distribution function in the presence of the solvent, we have

$$\beta F_{ab}(r) = -\beta \frac{du_{ab}(r)}{dr} = \frac{g'_{ab}(r)}{g_{ab}(r)}. \quad (3.3)$$

In MC simulations, we can calculate the force by means of

$$\beta F_{ab}(r) = -\sigma_{1b}^2 \left\langle \sum_i \int d\Omega_s \, \cos\theta_s \delta(\sigma_{1b}\widehat{\mathbf{s}} - \mathbf{s}_i) \right\rangle$$
$$\approx -3\sigma_{1b}^2 \left\langle \sum_i \frac{\Pi_{s_i - \frac{\epsilon}{2}, s_i + \frac{\epsilon}{2}}(\sigma_{1b}) \cos\theta_{s_i}}{\left(s_i + \frac{\epsilon}{2}\right)^3 - \left(s_i - \frac{\epsilon}{2}\right)^3} \right\rangle, \quad (3.4)$$

where the boxcar function $\Pi_{a,b}(x) = 1$ if $a \leq x < b$ and zero otherwise, ϵ is a discretization of the s variable, and in the second line of Eq. (3.4) we have discretized the radial part of the Dirac delta function. We can also rewrite Eq. (3.4), by neglecting the term in ϵ^3 in the denominator, as follows:

$$F_{ab}^*(r) \equiv \sigma_1 \beta F_{ab}(r) \approx -\sigma_1 I^{(r)}(\sigma_{1b}), \quad (3.5)$$

where $F_{ab}^*(r)$ is the dimensionless force and

$$I^{(r)}(s) = \left\langle \sum_i \frac{\Pi_{s - \frac{\epsilon}{2}, s + \frac{\epsilon}{2}}(s_i) \cos\theta_{s_i}}{\epsilon} \right\rangle. \quad (3.6)$$

In the simulations, $I^{(r)}(s)$ is evaluated at $s = s_\kappa = \sigma_{1b} + (2\kappa + 1)\epsilon/2$ with $\kappa = 0, 1, 2, \ldots$. The force $F_{ab}^*(r)$ is obtained by extrapolating the data at the contact value $s = \sigma_{1b}$.

2. Multicomponent solvent

In a multicomponent solvent, we have $\rho^{(r)}(\mathbf{q}) = \sum_\mu \rho_\mu^{(r)}(\mathbf{q})$ with $\rho_\mu^{(r)}(\mathbf{q}) = \langle \sum_i \delta_{\mu_i,\mu} \delta(\mathbf{q} - \mathbf{r}_i) \rangle$, where the Greek index stands for the species, the Roman index stands for the particle label, and μ_i denotes the species of particle i. The depletion force is now given by

$$\beta F_{ab}(r) = -\sum_\mu \sigma_{\mu b}^2 \int d\Omega_s \, \cos\theta_s \rho_\mu^{(r)}(\mathbf{r}_b + \sigma_{\mu b}\widehat{\mathbf{s}}). \quad (3.7)$$

The output from the MC simulations are the functions

$$I_\mu^{(r)}(s) = \left\langle \sum_i \delta_{\mu,\mu_i} \frac{\Pi_{s - \frac{\epsilon}{2}, s + \frac{\epsilon}{2}}(s_i) \cos\theta_{s_i}}{\epsilon} \right\rangle, \quad (3.8)$$

calculated at $s = s_\kappa = \sigma_{\mu b} + (2\kappa + 1)\epsilon/2$ with $\kappa = 0, 1, 2, \ldots$, so that we now have

$$F_{ab}^*(r) = \sigma_1 \beta F_{ab}(r) = -\sigma_1 \sum_\mu I_\mu^{(r)}(\sigma_{\mu b}). \quad (3.9)$$

B. Rational-function approximation

Within the RFA[7,27,28,37] one explicitly obtains the Laplace transform $G_{ab}(s)$ of $rg_{ab}(r)$ in the solute infinite-dilution limit ($x_a \to 0$ and $x_b \to 0$) of a quaternary mixture where the solvent is made of species 1 and 2 and the solute is made of species $a = 3$ and $b = 4$. Then, from Eq. (3.3) we have

$$\beta F_{ab}(r) = \frac{[rg_{ab}(r)]'}{rg_{ab}(r)} - \frac{1}{r}$$
$$= \frac{\mathcal{L}^{-1}[sG_{ab}(s) - e^{-\sigma_{ab}s}\sigma_{ab}g_{ab}(\sigma_{ab}^+)]}{\mathcal{L}^{-1}[G_{ab}(s)]} - \frac{1}{r}, \quad (3.10)$$

where $\mathcal{L}^{-1}$ stands for an inverse Laplace transform. In this equation, it is understood that $r > \sigma_{ab}$ since the force is of course singular in the region $0 \leq r \leq \sigma_{ab}$. Thus, given that $\mathcal{L}^{-1}[e^{-\sigma_{ab}s}] = \delta(r - \sigma_{ab})$, we may rewrite

$$\beta F_{ab}(r) = \frac{\mathcal{L}^{-1}[sG_{ab}(s)]}{\mathcal{L}^{-1}[G_{ab}(s)]} - \frac{1}{r}, \quad r > \sigma_{ab}. \quad (3.11)$$

As discussed in Ref. 27, the RFA inverse Laplace transforms for NAHS mixtures could in principle present a spurious behavior in the shell $\min(\sigma_{ab}, \tau_{ab}) \leq r \leq \max(\sigma_{ab}, \tau_{ab})$, where τ_{ab} is the minimum of the list of values $\sigma_{bk} - (\sigma_k - \sigma_a)/2$ ($k = 1$–4) that are different from σ_{ab}. In our case, however, since the solute-solvent interaction is additive, we have $\sigma_{bk} - (\sigma_k - \sigma_a)/2 = \sigma_{ab}$ for all k, so that $\tau_{ab} = \sigma_{ab}$ and the spurious behavior vanishes.

In the limit $\sigma_b/\sigma_a \to \infty$, the solute sphere b is felt as a planar hard wall by both a solvent particle and by the solute particle a. Before taking the limit we introduce the shifted radial distribution function $\gamma_{ab}(D) = g_{ab}(D + \sigma_{ab})$ for a surface-to-surface distance $D \geq 0$. In Laplace space,

$$G_{ab}(s) = e^{-\sigma_{ab}s}[\sigma_{ab}\Gamma_{ab}(s) - \Gamma'_{ab}(s)], \quad (3.12)$$

where $\Gamma_{ab}(s)$ is the Laplace transform of $\gamma_{ab}(D)$ and $\Gamma'_{ab}(s) = d\Gamma_{ab}(s)/ds$. In the wall limit, Eq. (3.12) yields

$$\Gamma_{aw}(s) = \lim_{\sigma_b/\sigma_a \to \infty} \frac{2}{\sigma_b} e^{\sigma_{ab}s} G_{ab}(s). \quad (3.13)$$

The corresponding expression for the depletion force is

$$\beta F_{aw}(D) = \frac{\gamma'_{aw}(D)}{\gamma_{aw}(D)} = \frac{\mathcal{L}^{-1}[s\Gamma_{aw}(s) - \gamma_{aw}(0)]}{\mathcal{L}^{-1}[\Gamma_{aw}(s)]}$$
$$= \frac{\mathcal{L}^{-1}[s\Gamma_{aw}(s)]}{\mathcal{L}^{-1}[\Gamma_{aw}(s)]}, \quad (3.14)$$

where in the last step we have taken into account that $D > 0$ and thus the term coming from $\mathcal{L}^{-1}[1] = \delta(D)$ can be ignored.

Appendix A gives some details on how to carry out the solute infinite-dilution limit analytically, while Appendix B shows how to subsequently carry out the wall limit. Once $G_{ab}(s)$ and $\Gamma_{aw}(s)$ are known, the inverse Laplace transforms may be carried out numerically following the recipe of Ref. 38. When the solvent nonadditivity is switched off ($\Delta = 0$) our RFA approach reduces to the usual PY approximation.[7,27]

The RFA for NAHS systems inherits from the PY approximation for AHS fluids the possibility of yielding nonphysical results near contact for the big-big correlation function in the case of strongly asymmetric mixtures.[39–41] As proposed by Henderson,[42] a simple and convenient way of circumventing this difficulty consists in the replacement $g \rightarrow \exp(g - 1)$. Thus, in order to correct the breakdown of the theory near solute contact, we have also considered an "exponential" RFA (exp-RFA) approximation where[21]

$$g_{ab}^{\text{exp-RFA}}(r) = \exp\left[g_{ab}^{\text{RFA}}(r) - 1 \right]. \quad (3.15)$$

IV. SIMULATION DETAILS

We performed canonical MC simulations in a parallelepipedal box ($-H/2 < x < H/2$, $-L/2 < y < L/2$, $-L/2 < z < L/2$) with periodic boundary conditions. The two solute spheres a and b are fixed in space, centered at $(-r/2, 0, 0)$ and $(r/2, 0, 0)$, respectively, as shown in Fig. 1. The solvent is in general a binary NAHS mixture, but we will always assume additivity between the solute and the solvent. According to the Metropolis algorithm,[43] a solvent particle move is rejected whenever it overlaps with another solvent particle or with any of the two solute spheres. The maximum random particle displacement was chosen so as to have acceptance ratios close to 50%. During the run we measured the shell integrals $I_\mu^{(r)}(s)$ of Eq. (3.8) and the local solvent density. We chose H and L large enough so that away from the two solute spheres the local solvent density shows a bulk-like plateau and thus the
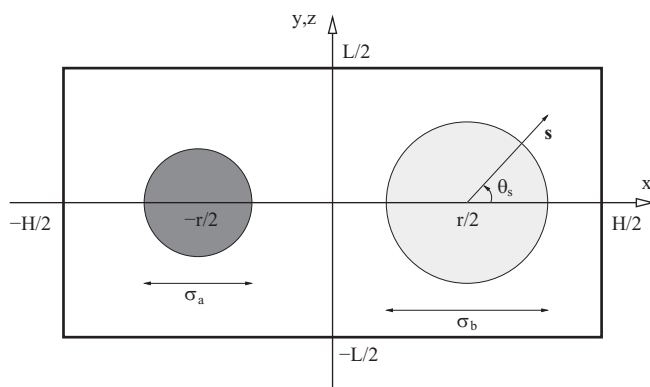

FIG. 1. Schematic simulation arrangement. The simulation box is the parallelepiped $-H/2 < x < H/2$, $-L/2 < y < L/2$, $-L/2 < z < L/2$ with periodic boundary conditions. H and L are chosen large enough so as to have a solvent density exhibiting a bulk-like plateau away from the two solute spheres.
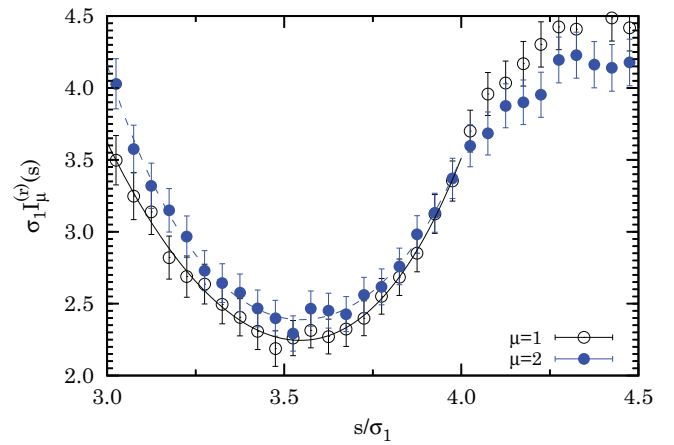

FIG. 2. Shell integrals $I_\mu^{(r)}(s)$ at $r/\sigma_1 = 5$ for the case $x_1 = \frac{1}{2}$, $\sigma_2/\sigma_1 = 1$, $\Delta = 0$, $\sigma_b/\sigma_a = 1$, $\sigma_a/\sigma_1 = 5$. Here, $H/\sigma_1 = 18$, $L/\sigma_1 = 12$, $N = 1134$. The bulk packing fraction is $\eta \approx 0.239(5)$ and the simulation time was $\tau = 4 \times 10^5 N$ single particle moves. The lines are least-square quartic fits on the interval $3 \le s/\sigma_1 \le 4$ used to extrapolate $I_\mu^{(r)}(s)$ at contact ($s/\sigma_1 = \sigma_{1b}/\sigma_1 = 3$). The estimated force is then found to be $F_{ab}^*(r) = -\sigma_1 \left[I_1^{(r)}(\sigma_{1b}) + I_2^{(r)}(\sigma_{2b}) \right] \approx -7.78(8)$. This case is close to the one in Fig. 6(b) of Ref. 33.

solvent density in a cubic cell of side ℓ centered at $(x, y, z) = (-H/2, L/2, L/2)$ can be accepted as a good estimate of the bulk density ρ.

A typical output for the shell integrals from a single simulation is shown in Fig. 2. The uncertainty on each measured value at a given s is determined as $\sqrt{\sigma_v^2 K/\tau}$ where τ is the number of single particle moves, σ_v^2 is the variance of the measures during the run, and K is an estimate of the correlation time of the sequence of measurements assumed as independent from s. In order to determine the depletion force according to Eq. (3.9), we need to find the contact values $I_\mu^{(r)}(\sigma_{\mu b})$. We do this with a least-square quartic fit of the shell integrals near contact, as shown in Fig. 2. Since the solvent binary mixture for the choice of the model parameters in Fig. 2 reduces to a one-component system, no partial demixing is possible, so that the $1 \leftrightarrow 2$ symmetry implies the consequent equality of the two shell integrals. This is reasonably well satisfied within the error estimates. The slight asymmetry observed in Fig. 2 favors one species or the other, in different runs, with equal probabilities.

In the study of the wall limit $\sigma_b/\sigma_a \rightarrow \infty$, we removed the periodic boundary conditions along the x direction and placed a hard wall at $x = -H/2$ and another one at $x = H/2$, rejecting solvent-particle moves producing an overlap with the walls. The solute sphere a was placed on the x axis at $x = -H/2 + D + \sigma_a/2$ and the depletion force felt by the solute impurity $\hat{\mathbf{x}} F_{wa}(D)$ was calculated as a function of $D > 0$. The solvent bulk density was evaluated in a cubic cell of side ℓ centered at $(x, y, z) = (D/2 + \sigma_a/2, L/2, L/2)$.

One can take into account the volume excluded to the solvent particles by the solutes to define a (nominal) average packing fraction $\bar{\eta} = \bar{\eta}_1 + \bar{\eta}_2$, where

$$\bar{\eta}_\mu = \frac{\frac{\pi}{6} N x_\mu \sigma_\mu^3}{HL^2 - \frac{\pi}{6}\left(\sigma_{\mu a}^3 + \sigma_{\mu b}^3\right)} \quad (4.1)$$

if σ_b/σ_a = finite and

$$\overline{\eta}_\mu = \frac{\frac{\pi}{6} N x_\mu \sigma_\mu^3}{(H - \sigma_\mu)L^2 - \frac{\pi}{6}\sigma_{\mu a}^3} \qquad (4.2)$$

if $\sigma_b/\sigma_a = \infty$.

In all the cases presented in Sec. V, we took $N = 500$ solvent particles, box sides $H/\sigma_1 = 18$, $L/\sigma_1 = 12$, a number $\tau = 1.4 \times 10^6 N$ of single particle moves, and a discretization step $\epsilon/\sigma_1 = 0.05$. The side of the cell employed to evaluate the bulk density was $\ell = \sigma_1$.

V. RESULTS

In this section, we present our results for four representative classes of systems: two symmetric solute impurities in a symmetric (class S) or asymmetric (class A) solvent, and a planar wall and a solute impurity in a symmetric (class wS) or asymmetric (class wA) solvent. For each class, we have considered three solvent nonadditivities: zero, positive, and negative. This will allow us to assess the effect of solvent nonadditivity on the depletion force between the impurity particles or between the impurity and the wall. The RFA predictions will be compared with our MC simulations. The parameters characterizing the 12 different systems are given in Table I. The last column gives the average packing fraction $\overline{\eta} = \overline{\eta}_1 + \overline{\eta}_2$ defined by Eqs. (4.1) (solute-solute systems) and (4.2) (wall-solute systems). In the asymmetric-solvent cases $(\sigma_2/\sigma_1 = \frac{3}{2})$, the value of the mole fraction $(x_1 = \frac{193}{250})$ has been chosen such that both species occupy practically equal volumes $(x_1\sigma_1^3/x_2\sigma_2^3 = 1.003)$.

As an illustration, Fig. 3 shows a snapshot of an equilibrated MC configuration of system S_0 with the two identical solute particles at contact.

A. Symmetric solvent and symmetric solute impurities

We first consider a symmetric $1 \leftrightarrow 2$ solvent (systems S_0, S_+, S_-). In general, for positive nonadditivity ($\Delta > 0$) and sufficiently high densities, the solvent may undergo demixing,[32] so that in the simulation we would get $I_1^{(r)}(s) \neq I_2^{(r)}(s)$ by spontaneous symmetry breaking. On the other

TABLE I. Values of the parameters defining the 12 systems considered in this work.

Label	σ_b/σ_a	σ_a/σ_1	x_1	σ_2/σ_1	Δ	$\overline{\eta}$
S_0	1	5	$\frac{1}{2}$	1	0	0.1021
S_+					$\frac{1}{4}$	
S_-					$-\frac{1}{4}$	
A_0	1	5	$\frac{193}{250}$	$\frac{3}{2}$	0	0.1576
A_+					$\frac{1}{5}$	
A_-					$-\frac{1}{5}$	
wS_0	∞	5	$\frac{1}{2}$	1	0	0.1076
wS_+					$\frac{1}{4}$	
wS_-					$-\frac{1}{4}$	
wA_0	∞	5	$\frac{193}{250}$	$\frac{3}{2}$	0	0.1685
wA_+					$\frac{1}{5}$	
wA_-					$-\frac{1}{5}$	

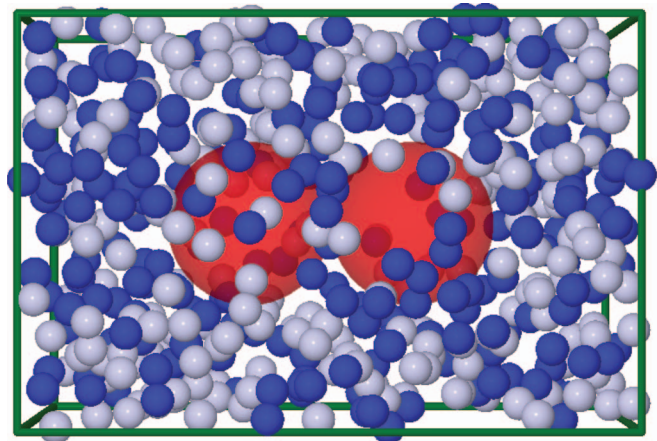FIG. 3. Snapshot of an equilibrated MC configuration of system S_0. The solutes are the two big red spheres while the solvent binary mixture is made of small light and dark blue spheres.

hand, if, at a given density, the positive nonadditivity is not too large, the solvent will be in a mixed state and the equality of the two shell integrals is expected. However, we found that, even in states with a mixed solvent in the bulk, the solvent may be partially demixed in the region between the two solute particles because of density compression effects.[35] This may be responsible for an asymmetry in the two shell integrals, which is expected to be maximal near a surface-to-surface distance of the two solute impurities equal to one solvent diameter. In order to avoid this effect, we chose a sufficiently small value for the nonadditivity (system S_+).

The first columns of Table II present the simulation results for the depletion force and for the bulk packing fraction of systems S_0, S_+, and S_- as functions of the surface-to-surface distance $D = r - \sigma_{ab}$. We observe that the bulk packing fraction is weakly dependent on D and on Δ, being slightly larger than the average value $\overline{\eta}$.

The MC results for the depletion force are compared with the semi-analytical RFA predictions in Fig. 4. We recall that the RFA theory reduces to the PY theory in the additive case ($\Delta = 0$), so the middle solid and dashed lines in Fig. 4 actually represent the PY and exp-PY predictions, respectively. As we can see, those curves for the additive system S_0 agree quite well with the simulation data at and beyond a surface-to-surface separation between the two solute impurities equal to half the solvent diameter, $D \gtrsim \sigma_1/2$. In that region, our RFA theory successfully accounts for the influence of the solvent nonadditivity on the depletion force. A specially good agreement is observed at $D = \sigma_1$, where the theory predicts a kink in the force stemming from the first spatial derivative of the solute-solute radial distribution function. On the other hand, a less satisfactory result is observed near contact of the impurities ($D < \sigma_1/2$), where both the PY (system S_0) and the RFA (systems S_+ and S_-) theories exhibit an artificial upward bending of the curves (instead of the correct quasilinear behavior), implying a force less attractive than it should be. This is, at least qualitatively, corrected by the exp-PY and exp-RFA versions of the theories. Another possible correction could be to develop the second-order RFA,[44] which is known to work well in the additive solvent case.[7]

TABLE II. MC results for the symmetric cases S_0, S_+, S_-, and the asymmetric cases A_0, A_+, A_- (see Table I). D is the surface-to-surface separation between the two solutes and η is the bulk packing fraction of the solvent.

	S_0		S_+		S_-		A_0		A_+		A_-	
D/σ_1	F_{ab}^*	η	F_{ab}^*	η	F_{ab}^*	η	F_{ab}^*	η	F_{ab}^*	η	F_{ab}^*	η
0.00	−2.35(3)	0.109(1)	−2.59(2)	0.108(1)	−2.22(2)	0.110(1)	−3.09(3)	0.167(1)	−3.39(3)	0.169(1)	−2.86(2)	0.168(1)
0.25	−1.71(2)	0.109(1)	−1.73(3)	0.109(1)	−1.59(2)	0.110(1)	−2.26(2)	0.166(1)	−2.43(4)	0.169(1)	−2.23(3)	0.171(1)
0.50	−1.03(2)	0.109(1)	−0.93(3)	0.109(1)	−1.01(3)	0.110(1)	−1.40(3)	0.168(1)	−1.33(3)	0.170(1)	−1.41(2)	0.169(1)
0.75	−0.30(3)	0.109(1)	−0.00(2)	0.109(1)	−0.40(2)	0.110(1)	−0.56(3)	0.169(1)	−0.24(3)	0.169(1)	−0.68(3)	0.170(1)
0.84	−0.03(2)	0.109(1)	0.25(3)	0.108(1)	−0.12(3)	0.110(1)	−0.22(3)	0.168(1)	0.13(3)	0.168(1)	−0.35(3)	0.169(1)
0.92	0.26(2)	0.109(1)	0.49(3)	0.108(1)	0.06(3)	0.110(1)	0.10(2)	0.168(1)	0.55(3)	0.168(1)	−0.10(3)	0.170(1)
1.00	0.36(3)	0.109(1)	0.66(3)	0.109(1)	0.21(3)	0.109(1)	0.45(2)	0.171(1)	0.95(4)	0.168(1)	0.17(2)	0.169(1)
1.08	0.32(4)	0.110(1)	0.63(4)	0.109(1)	0.27(3)	0.110(1)	0.50(4)	0.169(1)	0.76(6)	0.171(1)	0.15(4)	0.170(1)
1.16	0.17(4)	0.109(1)	0.28(3)	0.108(1)	0.08(3)	0.110(1)	0.21(4)	0.169(1)	0.36(5)	0.165(1)	0.03(3)	0.170(1)
1.25	−0.02(4)	0.109(1)	0.01(4)	0.108(1)	−0.02(3)	0.110(1)	0.07(5)	0.168(1)	0.23(4)	0.170(1)	−0.07(3)	0.170(1)
1.50	−0.01(4)	0.110(1)	0.02(4)	0.109(1)	−0.03(3)	0.110(1)	0.22(4)	0.169(1)	0.48(5)	0.166(1)	0.14(4)	0.170(1)
1.75	0.01(2)	0.109(1)	−0.13(4)	0.109(1)	−0.05(3)	0.109(1)	−0.07(4)	0.169(1)	−0.20(5)	0.168(1)	0.01(4)	0.170(1)
2.00	0.01(3)	0.109(1)	−0.11(3)	0.109(1)	−0.00(2)	0.110(1)	−0.10(3)	0.169(1)	−0.04(3)	0.168(1)	−0.02(3)	0.170(1)
2.25	−0.03(3)	0.109(1)	−0.06(3)	0.108(1)	−0.02(3)	0.110(1)	−0.04(3)	0.170(1)	−0.12(4)	0.171(1)	−0.06(3)	0.171(1)
2.50	0.02(2)	0.109(1)	0.04(2)	0.109(1)	−0.00(2)	0.109(1)	−0.00(3)	0.169(1)	0.09(3)	0.167(1)	−0.02(2)	0.169(1)

The positive nonadditivity enhances the depletion force and the negative nonadditivity inhibits it. These trends for the effect of the solvent nonadditivity on the depletion force could be expected from the following simple argument. To first order in density, the bulk compressibility factor of the solvent is $1 + B_2\rho$, with $B_2 = (2\pi/3)\sum_{i,j} x_i x_j \sigma_{ij}^3$ being the second virial coefficient. Therefore, in the low-density regime, one would expect the NAHS solvent with a packing fraction η to behave similarly to an effective AHS solvent with an effective packing fraction

$$\eta_{\text{eff}} = \eta \frac{\sum_{i,j} x_i x_j \sigma_{ij}^3}{\sum_{i,j} x_i x_j [(\sigma_i + \sigma_j)/2]^3}. \quad (5.1)$$

Thus, introducing a positive nonadditivity in the solvent is qualitatively analogous to increasing its density, which in turn produces an enhancement of the solute-solute depletion force. Of course, a negative nonadditivity produces the opposite effect.

B. Asymmetric solvent and symmetric solute impurities

Next, we consider the asymmetric-solvent systems A_0, A_+, and A_-. In those cases, the two shell integrals are obviously different, i.e., $I_1^{(r)}(s) \neq I_2^{(r)}(s)$. As before, we want to measure the effect on the depletion force of adding a certain nonadditivity to the solvent.

The MC values for the depletion force and the bulk packing fraction are given in Table II. As in the symmetric-solvent cases, the bulk packing fractions are slightly larger than the nominal average values, but now the influence of the solute-solute separation on the bulk values is more pronounced.

Figure 5 compares the MC and RFA results for systems A_0, A_+, and A_-. As in the symmetric case, RFA=PY for the AHS solvent ($\Delta = 0$). Now, in addition to a kink in the depletion force at $D = \sigma_1$, the RFA predicts a second kink at $D = \sigma_2$, with smooth oscillations around zero beyond that point. Again, the variation of the depletion force with distance
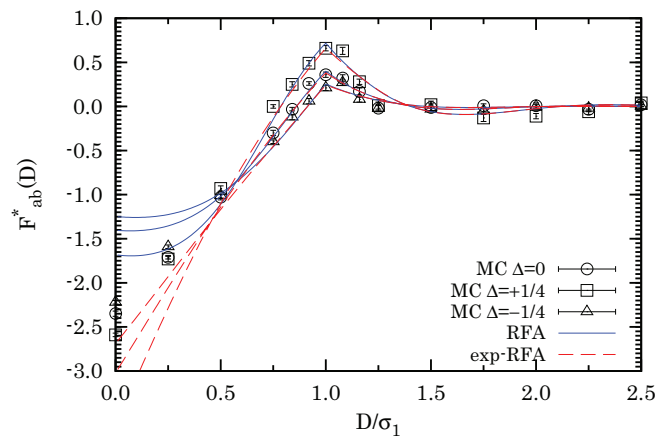

FIG. 4. Depletion force between two identical big hard spheres immersed in a solvent binary mixture of small hard spheres, as a function of their surface-to-surface separation, for systems S_0, S_+, and S_- (see Table I). The bulk packing fraction used to obtain the (exp-)RFA results was taken as $\eta = 0.109$ in all cases. The MC results are the ones of Table II.
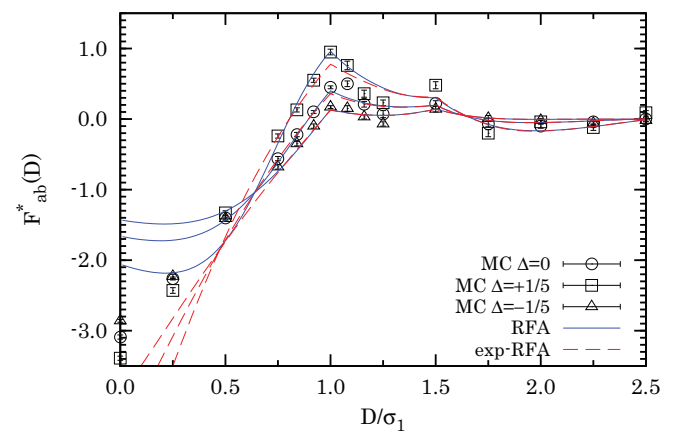

FIG. 5. Depletion force between two identical big hard spheres immersed in a solvent binary mixture of small hard spheres, as a function of their surface-to-surface separation, for systems A_0, A_+, and A_- (see Table I). The bulk packing fraction used to obtain the (exp-)RFA results was taken as $\eta = 0.170$ in all cases. The MC results are the ones of Table II.

TABLE III. MC results for the symmetric cases wS$_0$, wS$_+$, wS$_-$, and the asymmetric cases wA$_0$, wA$_+$, wA$_-$ (see Table I). D is the surface-to-surface separation between the wall and the solute sphere and η is the bulk packing fraction of the solvent.

	wS$_0$		wS$_+$		wS$_-$		wA$_0$		wA$_+$		wA$_-$	
D/σ_1	F_{aw}^*	η	F_{aw}^*	η	F_{aw}^*	η	F_{aw}^*	η	F_{aw}^*	η	F_{aw}^*	η
0.00	−4.44(3)	0.110(1)	−4.68(3)	0.108(1)	−4.10(2)	0.111(1)	−5.73(2)	0.172(1)	−6.20(2)	0.169(1)	−5.20(2)	0.170(1)
0.25	−3.29(2)	0.109(1)	−3.30(2)	0.108(1)	−3.11(2)	0.110(1)	−4.34(3)	0.168(1)	−4.49(3)	0.168(1)	−4.02(1)	0.172(1)
0.50	−1.99(2)	0.109(1)	−1.82(3)	0.108(1)	−2.01(2)	0.111(1)	−2.70(2)	0.171(1)	−2.55(3)	0.165(1)	−2.69(2)	0.171(1)
0.75	−0.66(2)	0.109(1)	−0.11(3)	0.108(1)	−0.79(3)	0.110(1)	−1.03(3)	0.170(1)	−0.32(4)	0.168(1)	−1.26(3)	0.172(1)
0.84	−0.06(2)	0.110(1)	0.60(3)	0.108(1)	−0.38(3)	0.111(1)	−0.30(3)	0.170(1)	0.56(3)	0.170(1)	−0.72(3)	0.172(1)
0.92	0.42(3)	0.109(1)	1.06(3)	0.108(1)	0.05(2)	0.110(1)	0.28(3)	0.169(1)	1.24(3)	0.169(1)	−0.22(3)	0.172(1)
1.00	0.95(3)	0.110(1)	1.66(2)	0.108(1)	0.59(3)	0.110(1)	1.00(3)	0.168(1)	2.01(3)	0.167(1)	0.34(3)	0.171(1)
1.08	0.83(5)	0.109(1)	1.42(6)	0.108(1)	0.52(4)	0.110(1)	0.92(7)	0.168(1)	1.91(10)	0.165(1)	0.43(5)	0.172(1)
1.16	0.33(5)	0.109(1)	0.44(7)	0.108(1)	0.19(4)	0.110(1)	0.41(8)	0.168(1)	0.99(10)	0.168(1)	0.16(5)	0.172(1)
1.25	−0.06(5)	0.110(1)	0.04(7)	0.109(1)	−0.05(5)	0.110(1)	0.11(8)	0.169(1)	0.54(10)	0.167(1)	−0.04(7)	0.171(1)
1.50	0.08(6)	0.110(1)	−0.02(7)	0.109(1)	0.12(5)	0.110(1)	0.55(7)	0.171(1)	0.93(9)	0.165(1)	0.38(7)	0.172(1)
1.75	−0.06(5)	0.109(1)	−0.17(6)	0.109(1)	−0.07(4)	0.110(1)	−0.15(7)	0.170(1)	−0.56(8)	0.167(1)	−0.07(6)	0.171(1)
2.00	−0.00(2)	0.110(1)	−0.06(3)	0.108(1)	0.01(2)	0.110(1)	−0.04(5)	0.171(1)	−0.28(5)	0.167(1)	−0.02(3)	0.171(1)
2.25	−0.03(3)	0.109(1)	0.05(3)	0.108(1)	0.00(2)	0.110(1)	−0.05(4)	0.168(1)	−0.16(4)	0.167(1)	−0.00(3)	0.172(1)
2.50	0.05(2)	0.109(1)	0.03(3)	0.108(1)	−0.03(2)	0.111(1)	0.07(3)	0.170(1)	−0.01(3)	0.165(1)	0.01(2)	0.172(1)

increases (decreases) if a positive (negative) nonadditivity is included, as expected from the argument behind Eq. (5.1). Analogous to Fig. 4, a reasonable agreement between our theoretical approximation and the simulation results is observed for $D \gtrsim \sigma_1/2$, but the agreement breaks down when the solutes are near contact. On the other hand, the exp-RFA approximation has the correct linear behavior near contact, even if it underestimates the contact values. Note also that, while RFA and exp-RFA are practically indistinguishable for $D \gtrsim \sigma_1/2$ in Fig. 4, both approximations are slightly different in the region near the kink at $D = \sigma_1$ in the case A$_+$, RFA being more accurate than exp-RFA.

C. A wall and one solute impurity in a symmetric solvent

We now explore the cases of extreme solute asymmetry in the limit $\sigma_b/\sigma_a \to \infty$, where sphere b becomes a planar hard wall.

We start with the cases of a symmetric solvent (systems wS$_0$, wS$_+$, and wS$_-$). The MC data for the depletion force and the bulk packing fraction are listed in the first columns of Table III. Since the solvents in systems wS$_0$, wS$_+$, and wS$_-$ are in the same bulk state (except for small changes of η) as in systems S$_0$, S$_+$, and S$_-$, respectively, we can test the Derjaguin approximation[45] $F_{aa}^*(D) \approx \frac{1}{2} F_{aw}^*(D)$. As can be seen from comparison of Tables II and III, the Derjaguin approximation is rather well satisfied in our simulations, even in the cases of NAHS solvents, $\frac{1}{2} F_{aw}^*(D)$ being typically 1%–10% smaller than $F_{aa}^*(D)$.

Theory and simulation are compared in Fig. 6. Not surprisingly, our RFA approximation (which is again equivalent to the PY approximation in the case $\Delta = 0$) performs quite well for $D \gtrsim \sigma_1/2$ but it breaks down near contact between the wall and the solute spherical impurity, this effect being now more important than in the cases of two identical solutes (Fig. 4). On the other hand, the exp-RFA approximation ex-

hibits a better (quasilinear) behavior near contact, although it underestimates the contact values. Also, analogous to what is observed in Fig. 5, exp-RFA is less accurate than RFA near the kink at $D = \sigma_1$ when a positive nonadditivity is present.

D. A wall and one solute impurity in an asymmetric solvent

To complete the picture, we finally consider the wall-solute force in a NAHS solvent (systems wA$_0$, wA$_+$, and wA$_-$). The corresponding MC data can be found in Table III. The Derjaguin approximation $F_{aa}^*(D) \approx \frac{1}{2} F_{aw}^*(D)$ is again well satisfied, although the deviations are slightly larger than in the wS cases, $\frac{1}{2} F_{aw}^*(D)$ being about 4%–10% smaller than $F_{aa}^*(D)$.

As Fig. 7 shows, in contrast to the cases S$_+$, A$_+$, and wS$_+$ plotted in Figs. 4–6, respectively, the RFA for a positive
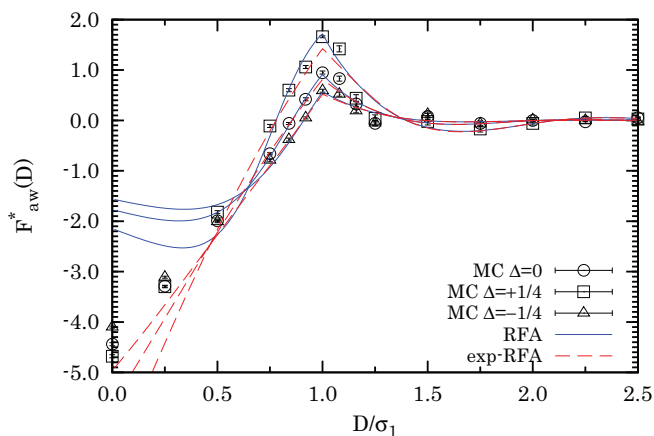

FIG. 6. Depletion force between a hard wall and a big hard sphere immersed in a solvent binary mixture of small hard spheres, as a function of their surface-to-surface separation, for systems wS$_0$, wS$_+$, and wS$_-$ (see Table I). The bulk packing fraction used to obtain the (exp-)RFA results was taken as $\eta = 0.109$ in all cases. The MC results are the ones of Table III.
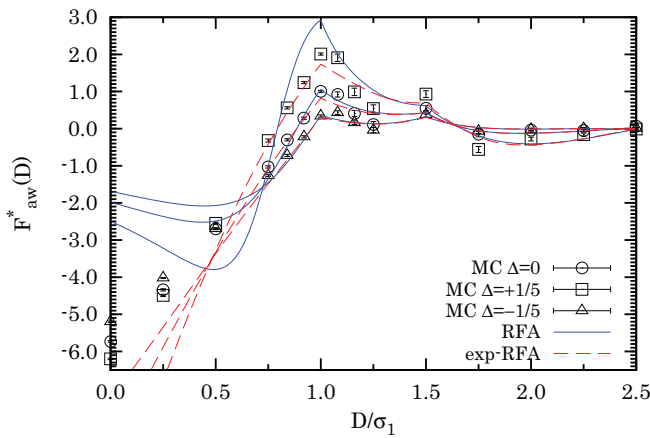
FIG. 7. Depletion force between a hard wall and a big hard sphere immersed in a solvent binary mixture of small hard spheres, as a function of their surface-to-surface separation, for systems wA$_0$, wA$_+$, and wA$_-$ (see Table I). The bulk packing fraction used to obtain the (exp-)RFA results was taken as $\eta = 0.170$ in all cases. The MC results are the ones of Table III.

nonadditivity (system wA$_+$) is not able to capture accurately the values of the depletion force in the region near the first kink at $D = \sigma_1$, while the related approximation exp-RFA does. Moreover, the artificial upward bend of the PY curve ($\Delta = 0$) and of the two RFA curves ($\Delta = \pm\frac{1}{5}$) in the region $D \lesssim \sigma_1/2$ is much more dramatic than in Figs. 4–6. Again, the exp-RFA lines tend to correct this behavior but they underestimate the contact values.

VI. CONCLUSIONS

We have studied in this paper the mutual depletion force acting on two solute hard spheres immersed in a solvent consisting in a binary NAHS mixture. We have employed two complementary tools: canonical MC simulations and the semi-analytical RFA (which is fully equivalent to the PY solution when the solvent nonadditivity is switched off). Four different settings have been considered: two symmetric solutes in a symmetric and in an asymmetric solvent, and two extremely asymmetric solutes (in the limit where one of the two spheres reduces to a planar hard wall) again in a symmetric and in an asymmetric solvent. For each class of systems, we have chosen three possibilities: zero nonadditivity, positive nonadditivity, and negative nonadditivity. In all the systems, the solvent remained in a mixed state.

We have found that the RFA performs reasonably well in all cases for a surface-to-surface distance D greater than the radius of the smallest solvent particles, except in the case wA$_+$ of a wall with an asymmetric solvent with positive nonadditivity, where the theory overestimates the height of the first kink. The approximation in all cases breaks down at and near contact ($D = 0$). To correct this, we have also considered an exp-RFA, which shows the correct quasilinear behavior near contact, even if it is still not able to quantitatively capture the contact values. The approximations correctly predict kinks in the depletion force when D equals any of the two solvent diameters. Our results show how in all cases a positive solvent nonadditivity enhances the depletion force whereas a

negative one inhibits it. Moreover, the Derjaguin approximation is well satisfied in our simulations, even for the nonadditive solvent.

As possible further developments of our study, we plan to try to correct the theoretical approximation near contact and to study the behavior of the force as one approaches the demixing transition of the solvent on the critical isochore.

APPENDIX A: THE SOLUTE INFINITE-DILUTION LIMIT IN THE RFA

For convenience, we here use Roman indexes for the species instead of Greek indexes as done in the main text. In Ref. 27, the following proposal for the structural properties of an n-component NAHS fluid defined through the Laplace transform $G_{ij}(s)$ of $rg_{ij}(r)$ was given:

$$G_{ij}(s) = s^{-2} \sum_{k=1}^{n} e^{-\sigma_{ik}s} L_{ik}(s) B_{kj}(s), \qquad \text{(A1)}$$

with

$$\mathsf{B}^{-1}(s) = \mathsf{I} - \mathsf{A}(s), \qquad \text{(A2)}$$

$$A_{ij}(s) = \frac{2\pi\rho x_i}{s^3} \left[N_{ij}(s)e^{a_{ij}s} - L_{ij}(s)e^{-\sigma_{ij}s} \right], \qquad \text{(A3)}$$

where I is the unit matrix,

$$L_{ij}(s) \equiv L_{ij}^{(0)} + L_{ij}^{(1)}s, \qquad \text{(A4)}$$

$$N_{ij}(s) \equiv L_{ij}^{(0)} \left(1 - b_{ij}s + \frac{b_{ij}^2 s^2}{2} \right) + L_{ij}^{(1)}s(1 - b_{ij}s), \quad \text{(A5)}$$

$$b_{ij} \equiv \sigma_{ij} + a_{ij}, \quad a_{ij} \equiv \frac{1}{2}(\sigma_i - \sigma_j). \qquad \text{(A6)}$$

Equations (A1)–(A5) provide the explicit s-dependence of the Laplace transform $G_{ij}(s)$, but it still remains to determine the two sets of parameters $L_{ij}^{(0)}$ and $L_{ij}^{(1)}$. This is done by enforcing the physical requirements[27] $\lim_{s \to 0} s^2 G_{ij}(s) = 1$ and $\lim_{s \to 0} s^{-1}[s^2 G_{ij}(s) - 1] = 0$. The results are

$$L_{ij}^{(0)} = S_j, \quad L_{ij}^{(1)} = T_j + \sigma_{ij} S_j, \qquad \text{(A7)}$$

where

$$S_j \equiv \frac{1 - \pi\rho\Psi_j}{\left(1 - \pi\rho\Lambda_j\right)\left(1 - \pi\rho\Psi_j\right) - \pi^2\rho^2\mu_{j|2,0}\Omega_j}, \quad \text{(A8)}$$

$$T_j \equiv \frac{\pi \rho \Omega_j}{(1 - \pi \rho \Lambda_j)(1 - \pi \rho \Psi_j) - \pi^2 \rho^2 \mu_{j|2,0} \Omega_j}, \quad \text{(A9)}$$

$$\Lambda_j \equiv \mu_{j|2,1} - \frac{1}{3} \mu_{j|3,0}, \quad \text{(A10)}$$

$$\Psi_j \equiv \frac{2}{3} \mu_{j|3,0} - \mu_{j|2,1}, \quad \text{(A11)}$$

$$\Omega_j \equiv \mu_{j|3,1} - \mu_{j|2,2} - \frac{1}{4} \mu_{j|4,0}, \quad \text{(A12)}$$

and we have called

$$\mu_{j|p,q} \equiv \sum_{k=1}^{n} x_k b_{kj}^p \sigma_{kj}^q. \quad \text{(A13)}$$

We now choose our quaternary mixture ($n = 4$) in such a way that the first two species ($i = 1$ and $i = 2$) describe the solvent and the last two species ($i = 3 = a$ and $i = 4 = b$) describe the solute. Then, in the infinite-dilution limit $x_a \to 0$ and $x_b \to 0$ we have that

$$\mathbf{B}^{-1} = \begin{pmatrix} (\mathbf{B}^{-1})_{11} & (\mathbf{B}^{-1})_{12} & -A_{1a} & -A_{1b} \\ (\mathbf{B}^{-1})_{21} & (\mathbf{B}^{-1})_{22} & -A_{2a} & -A_{2b} \\ 0 & 0 & 1 & 0 \\ 0 & 0 & 0 & 1 \end{pmatrix}, \quad \text{(A14)}$$

and thus

$$\mathbf{B} = \begin{pmatrix} B_{11} & B_{12} & C_{1a} & C_{1b} \\ B_{21} & B_{22} & C_{2a} & C_{2b} \\ 0 & 0 & 1 & 0 \\ 0 & 0 & 0 & 1 \end{pmatrix}, \quad \text{(A15)}$$

where

$$C_{ij} = \sum_{k=1}^{2} B_{ik} A_{kj}, \quad i = 1, 2 \text{ and } j = a, b. \quad \text{(A16)}$$

We have reduced the inversion of the original 4×4 matrix $\mathbf{B}^{-1}$ to the inversion of just the 2×2 submatrix corresponding to the solvent.

We then find

$$s^2 G_{ab}(s) = e^{-\sigma_{ab}s} L_{ab}(s) + \sum_{k=1}^{2} e^{-\sigma_{ak}s} L_{ak}(s) C_{kb}(s), \quad \text{(A17)}$$

where now $\mu_{j|p,q} = \sum_{k=1}^{2} x_k b_{kj}^p \sigma_{kj}^q$.

APPENDIX B: THE WALL LIMIT IN THE RFA

Taking the limit $\sigma_b \to \infty$, we find from Eq. (A17),

$$\Gamma_{aw}(s) = \lim_{\sigma_b \to \infty} \frac{2}{\sigma_b} e^{\sigma_{ab}s} G_{ab}(s)$$

$$= \frac{2}{s^2} \left[\widetilde{L}_{aw}(s) + \sum_{k=1}^{2} L_{ak}(s) \widetilde{C}_{kw}(s) \right], \quad \text{(B1)}$$

where

$$\widetilde{L}_{aw}(s) \equiv \lim_{\sigma_b \to \infty} \frac{L_{ab}(s)}{\sigma_b}, \quad \text{(B2)}$$

$$\widetilde{C}_{kw}(s) \equiv \lim_{\sigma_b \to \infty} \frac{e^{a_{kb}s} C_{kb}(s)}{\sigma_b}, \quad k = 1, 2. \quad \text{(B3)}$$

[1]M. Dijkstra, R. van Roij, and R. Evans, Phys. Rev. Lett. **82**, 117 (1999).
[2]R. Roth, R. Evans, and A. A. Louis, Phys. Rev. E **64**, 051201 (2001).
[3]A. A. Louis and R. Roth, J. Phys.: Condens. Matter **13**, L777 (2001).
[4]C. D. Estrada-Alvarez, E. López-Sánchez, G. Pérez-Ángel, P. González-Mozuelos, J. M. Méndez-Alcaraz, and R. Castañeda Priego, J. Chem. Phys. **140**, 026101 (2014).
[5]S. Asakura and F. Oosawa, J. Chem. Phys. **22**, 1255 (1954).
[6]R. Roth, R. Evans, and S. Dietrich, Phys. Rev. E **62**, 5360 (2000).
[7]S. B. Yuste, A. Santos, and M. López de Haro, J. Chem. Phys. **128**, 134507 (2008); **140**, 179901 (2014).
[8]D. J. Ashton, N. B. Wilding, R. Roth, and R. Evans, Phys. Rev. E **84**, 061136 (2011).
[9]R. Castañeda-Priego, A. Rodríguez-López, and J. M. M. Alcaraz, J. Phys.: Condens. Matter **15**, S3393 (2003).
[10]T. Biben, P. Bladon, and D. Frenkel, J. Phys.: Condens. Matter **8**, 10799 (1996).
[11]P. Germain and S. Amokrane, Phys. Rev. Lett. **102**, 058301 (2009).
[12]M. Sikorski, A. R. Sandy, and S. Narayanan, Phys. Rev. Lett. **106**, 188301 (2011).
[13]P.-M. König, R. Roth, and S. Dietrich, Phys. Rev. E **74**, 041404 (2006).
[14]W. Li, T. Yang, and H. Ma, J. Chem. Phys. **128**, 044910 (2008).
[15]D. Henderson, A. D. Trokhymchuk, and D. T. Wasan, J. Mol. Liq. **112**, 21 (2004).
[16]R. Roth and M. Kinoshita, J. Chem. Phys. **125**, 084910 (2006).
[17]Y. Mao, J. Phys. II **5**, 1761 (1995).
[18]X. L. Chu, A. D. Nikolov, and D. T. Wasan, Langmuir **12**, 5004 (1996).
[19]S. A. Egorov, Phys. Rev. E **70**, 031402 (2004).
[20]G. Cinacchi, Y. Martínez-Ratón, L. Mederos, G. Navascués, A. Tani, and E. Velasco, J. Chem. Phys. **127**, 214501 (2007).
[21]A. Lajovic, M. Tomšič, and A. Jamnik, J. Chem. Phys. **130**, 104101 (2009).
[22]A. Jamnik, J. Chem. Phys. **131**, 164111 (2009).
[23]C. Bauer, T. Bieker, and S. Dietrich, Phys. Rev. E **62**, 5324 (2000).
[24]C. Hertlein, L. Heden, A. Gambassi, S. Dietrich, and C. Bechinger, Nature (London) **451**, 172 (2007).
[25]N. Gnan, E. Zaccarelli, P. Tartaglia, and F. Sciortino, Soft Matter **8**, 1991 (2012).
[26]N. Gnan, E. Zaccarelli, and F. Sciortino, J. Chem. Phys. **137**, 084903 (2012).
[27]R. Fantoni and A. Santos, Phys. Rev. E **84**, 041201 (2011). Note that in Eq. (2.12) the hats on the partial correlation functions should be replaced by tildes.
[28]R. Fantoni and A. Santos, Phys. Rev. E **87**, 042102 (2013).
[29]J. L. Lebowitz, Phys. Rev. **133**, A895 (1964).
[30]S. B. Yuste, A. Santos, and M. López de Haro, J. Chem. Phys. **108**, 3683 (1998).
[31]T. Biben and J.-P. Hansen, Phys. Rev. Lett. **66**, 2215 (1991).
[32]A. Santos, M. López de Haro, and S. B. Yuste, J. Chem. Phys. **132**, 204506 (2010).
[33]R. Dickman, P. Attard, and V. Simonian, J. Chem. Phys. **107**, 205 (1997).
[34]E. Allahyarov and H. Löwen, Phys. Rev. E **63**, 041403 (2001).
[35]P. Attard, J. Chem. Phys. **91**, 3083 (1989).
[36]R. Roth and R. Evans, Europhys. Lett. **53**, 271 (2001).
[37]S. B. Yuste, M. López de Haro, and A. Santos, Phys. Rev. E **53**, 4820 (1996).
[38]J. Abate and W. Whitt, Queueing Syst. **10**, 5 (1992).
[39]A. Jamnik, D. Bratko, and D. J. Henderson, J. Chem. Phys. **94**, 8210 (1991).
[40]A. Jamnik, J. Chem. Phys. **105**, 10511 (1996).
[41]D. Henderson and M. Lozada-Cassou, J. Colloid Interface Sci. **114**, 180 (1986).
[42]D. Henderson, J. Colloid Interface Sci. **121**, 486 (1988).
[43]M. H. Kalos and P. A. Whitlock, *Monte Carlo Methods* (John Wiley and Sons, New York, 1986).
[44]M. López de Haro, S. B. Yuste, and A. Santos, in *Theory and Simulation of Hard-Sphere Fluids and Related Systems*, Lectures Notes in Physics Vol. 753, edited by A. Mulero (Springer-Verlag, Berlin, 2008), pp. 183–245.
[45]B. V. Derjaguin, Kolloid Z. **69**, 155 (1934).